



Published in final edited form as:

Angew Chem Int Ed Engl. 2008 ; 47(38): 7284–7288. doi:10.1002/anie.200801810.

## Micellar Hybrid Nanoparticles for Simultaneous Magneto-Fluorescent Imaging and Drug Delivery\*\*

**Ji-Ho Park,**

Materials Science and Engineering Program, Department of Chemistry and Biochemistry, University of California, San Diego, 9500 Gilman, La Jolla, CA 92093 (USA)

**Geoffrey von Maltzahn,**

Harvard-MIT Division of Health Sciences and Technology, Massachusetts Institute of Technology, 77 Massachusetts Avenue, Cambridge, MA 02139 (USA)

**Erkki Ruoslahti,**

Burnham Institute for Medical Research at UCSB, University of California, Santa Barbara, 1105 Life Sciences Technology Bldg, Santa Barbara, CA 93106 (USA)

**Sangeeta N. Bhatia,** and

Harvard-MIT Division of Health Sciences and Technology, Massachusetts Institute of Technology, 77 Massachusetts Avenue, Cambridge, MA 02139 (USA)

**Michael J. Sailor\***

Materials Science and Engineering Program, Department of Chemistry and Biochemistry, University of California, San Diego, 9500 Gilman, La Jolla, CA 92093 (USA)

### Keywords

biological imaging; cancer; drug delivery; magnetic nanoparticles; micelle; quantum dots

Multifunctional nanoparticles have the potential to integrate therapeutic and diagnostic functions into a single nanodevice.<sup>[1–9]</sup> To date, several types of hybrid nanosystems containing multiple different types of nanoparticles have been developed that allow multimodal imaging. For example, formulations containing quantum dots (QD) and magnetic iron oxide nanoparticles (MN) provide a means to perform simultaneous fluorescent optical imaging and magnetic resonance imaging (MRI).<sup>[10–15]</sup> While these nanocomposites have been used for *in vitro* magnetic cell separation and *in vitro* cell targeting, there are limited *in vivo* studies, particularly for cancer imaging and therapy, due to poor stability or short systemic circulation times generally observed for these more complicated nanostructures.<sup>[16, 17]</sup> Herein, we introduce long-circulating, micellar hybrid nanoparticles (MHN) that contain MN, QD, and the anti-cancer drug doxorubicin (DOX) within a single

\*\*This project has been funded in part with Federal funds from the National Cancer Institute of the National Institutes of Health (Contract No. R01CA124427-02 and U01 HL 080718). M.J.S., E.R., and S.N.B. are members of the Moores UCSD Cancer Center and the UCSD NanoTUMOR Center under which this research was conducted and partially supported by NIH Grant U54 CA 119335. J.P. thanks the Korea Science and Engineering Foundation (KOSEF) for a Graduate Study Abroad Scholarship. The authors thank Dr. Edward Monosov for assistance with TEM analysis.

\*msailor@ucsd.edu.

polyethylene glycol (PEG)-phospholipid micelle and provide the first examples of simultaneous targeted drug delivery and dual-mode NIR-fluorescent and MR imaging of diseased tissue *in vitro* and *in vivo*.

Micellar preparations of hydrophobic drugs and nanoparticles using diblock polymers hold great potential for biomedical applications.<sup>[18–24]</sup> Such micellar coatings can display excellent stability, reducing the cytotoxicity of the hydrophobic drug or nanoparticle contents. Previous *in vitro* studies have demonstrated that drug molecules and MN can be incorporated within a micelle, allowing the corroboration of drug delivery by MRI.<sup>[21, 23]</sup> Furthermore, micellar preparations containing single-component nanomaterials such as QD and carbon nanotubes have been shown to be sufficiently stable for *in vivo* applications.<sup>[18, 24]</sup>

The synthesis of MHN is derived from a previously reported method for micellar encapsulation of QD.<sup>[18]</sup> Briefly, spherical oleic-acid coated MN with a size of 11 nm and elongated TOP-coated QD with a longitudinal size of 10–12 nm and NIR emission wavelength were encapsulated simultaneously within a micelle composed of a PEG-modified phospholipid, (Scheme 1). The MHN were removed from the micellar MN (MMN), micellar QD (MQD) and empty micelle byproducts produced in the synthesis by magnetic separation and centrifugation. Transmission electron microscope images and dynamic light scattering measurements reveal that the MHN consist of clusters of both MN and QD within a micellar coating with a hydrodynamic size of 60–70 nm (Figure 1a–d). The MN:QD ratio within the individual micelles can be adjusted by changing the mass ratio of MN to QD during the synthesis. By contrast, MMN or MQD prepared by encapsulating either MN or QD alone with PEG-phospholipids appear to be either individually encapsulated or encapsulated as dimers, respectively (Figure 1e and 1f). When relatively concentrated solutions (> 2 mg/mL) of MN and QD are added to the PEG-phospholipid solution during micelle formation, aggregates rather than isolated nanoparticles are observed to form. All preparations that produced concentrations of ~ 1 mg/mL MHN were stable in deionized water or in phosphate buffered saline (PBS) solutions, with no observable aggregation or dissociation for at least 1 month. Unlike dispersed arrangements of MN and QD reported in previous hybrid systems,<sup>[13, 14]</sup> the MN and QD in the MHN appear to be closely packed within a single micelle, similar to the clustering of MN that have been observed inside poly(caprolactone)-PEG copolymer systems.<sup>[22]</sup>

To examine the ability to remotely image MHN preparations, fluorescence spectra were measured using blue (450 nm) and NIR (680 nm) excitation (Figure 2). In both cases, as the ratio of MN to QD within a micelle increases, the intensity of fluorescence from the MHN assembly decreases with no significant spectral shift or line broadening of the emission spectrum observed. The loss of fluorescence intensity can be attributed to a decreased number of QD per micelle and to optical absorption by the MN, consistent with previous observations.<sup>[13, 14]</sup> Additionally, the proximity of MN and other QD in the MHN is likely to cause fluorescence quenching through non-radiative energy or charge transfer.<sup>[10, 25]</sup> Despite the quenching, fluorescence is intense enough to allow detection of MHN at sub-nanomolar QD concentrations. These inorganic QD-containing hybrid systems can be

excited and observed in the NIR spectral region with high photostability,<sup>[26, 27]</sup> providing significant advantages over MN labeled with organic fluorophores.<sup>[28, 29]</sup>

The MHN materials can also be imaged with MRI. The MR characteristics of MHN with varying MN:QD ratios were compared to MMN (Figure 2b and 2c). The  $T_2$ -weighted images of MHN1 and MHN3, containing MN clusters, display significantly larger MR contrast compared to MMN which contain only a single MN ( $T_2$  relaxation rates  $R_2 = 244.9$ , 187.5, and 104.9  $\text{mMFe}^{-1}\text{S}^{-1}$ , respectively). The increased  $T_2$  relaxivity for coalesced MN has been observed in several previous studies,<sup>[2, 22, 30]</sup> and it highlights an unexpected benefit of co-encapsulating both materials that is not observed in nanohybrids containing single MN.<sup>[5, 28, 31, 32]</sup> SQUID magnetic measurements confirm that MHN retain the superparamagnetic characteristics of individual MN (see Supporting Information, Figure S1). The MHN are thus detectable via both MRI and fluorescence at sub-micromolar Fe and sub-nanomolar QD concentrations (Figure 2b), highlighting their utility for bimodal applications.

The ability of MHN to target and dual-mode image tumor cells was tested on MDA-MB-435 human cancer cells. To allow the nanoassemblies to specifically target tumor cells, the MHN were conjugated with the targeting ligand F3, a peptide known to target cell-surface nucleolin in endothelial cells in tumor blood vessels and in tumor cells and to become internalized into these cells<sup>[33, 34]</sup>. This peptide is capable of transporting payloads such as nanoparticles or oligonucleotides into tumor vasculature *in vivo*<sup>[35–37]</sup>. Cells incubated with F3-conjugated MHN (F3-MHN) display dramatically increased NIR fluorescence and MRI contrast while cells incubated with unmodified MHN exhibit no significant fluorescence or MRI contrast (Figure 3a and 3b).

Simultaneous imaging and drug delivery was demonstrated using the anti-cancer drug DOX, which was incorporated into MHN during synthesis ( $\sim 0.093$  mg of DOX per mg of MHN, see Supporting Information, Figure S2). The intrinsic fluorescence of DOX allows the independent imaging of both DOX and QD contained in the MHN, which are observed to co-localize in some areas of MDA-MB-435 cells *in vitro* after 2 h of incubation (Figure 3c). During a 24-h period, F3-MHN were observed to chaperone DOX into cancer cells and release it endosomally into the nuclei following tumor cell internalization (Inset in Figure 3c, see Supporting Information, Figure S3). After 30 min of incubation with DOX-loaded F3-MHN (DOX-MHN-F3), the DOX fluorescence signal appeared mainly in the cytoplasm and co-localized with endosomes, whereas when free DOX was added, almost all of the DOX fluorescence signal was observed in the cell nuclei. As incubation time increased, the DOX in the cytoplasm was observed to translocate into the nuclei.

Although they are composed of relatively toxic QDs, no significant toxicity of the MHN assemblies was observed in this study, consistent with previous *in vitro* and *in vivo* studies with MQD and liposomal hybrid particles containing QD and MN.<sup>[17, 18]</sup> By contrast, DOX-incorporated F3-MHN display cytotoxicity which is significantly greater than that of equivalent quantities of free DOX or DOX-incorporated untargeted MHN (see Supporting Information Figure S4).

We next investigated the utility of MHN for multimodal *in vivo* imaging applications. We synthesized MHN containing QD that emit at a wavelength of 800 nm [MHN(800)]. This NIR wavelength is appropriate for imaging of organs *in vivo* and *ex vivo* because it maximizes tissue penetration while minimizing optical absorption by physiologically abundant species such as hemoglobin (see Supporting Information, Figure S5).<sup>[38]</sup> We find that these PEG-coated MHN exhibit substantial blood circulation times (~3 h half-life), comparable to other PEG-nanomaterial formulations (0.5~2 h half-life for PEGylated carbon nanotubes and 0.2~2.2 h for PEGylated QD).<sup>[24, 39, 40]</sup> We confirmed that MHN survive circulation in the blood stream without dissociation into individual MN or QD by TEM (see Supporting Information, Figure S6a).

Long-circulating nanoparticles in the size range of 20–200 nm have been shown to accumulate preferentially at tumor sites through an enhanced permeability and retention effect.<sup>[41, 42]</sup> Nude mice bearing MDA-MB-435 tumors were imaged prior to injection of MHN and then 20 h after injection. In these optical images, significant fluorescence was observed in the tumors 20 h after MHN injection (Figure 4a). Biodistribution measurements indicate that MHN mainly accumulate in the liver, while the quantity of MHN observed in other organs is not significant (see Supporting Information, Figure S6b). To evaluate the efficacy of combined MR and optical imaging, the tumors were harvested 20 h after injection and immediately imaged with a 4.7T MRI scanner and with a NIR optical imaging system. Significant differences in both fluorescence and MRI contrast, were observed between tumors injected with PBS and those injected with MHN (Figure 4b and see Supporting Information, Figure S6c). The differences observed in the fluorescence images are much more substantial than in the MR images, due to the low background signals associated with NIR imaging. Although these *in vivo* results are preliminary, the data provide promise for further *in vivo* applications due to the prolonged residence time in blood circulation displayed by MHN relative to similar liposomal hybrid systems<sup>[17]</sup>

In summary, micellar hybrid nanoparticles that contain MN, QD, and anti-cancer drug DOX within a single PEG-modified phospholipid micelle have been prepared. The hydrophobic chains of the PEG-phospholipids interact strongly with hydrophobic chains attached to the MN and QD, providing high dispersibility and stability for *in vitro* and *in vivo* applications. The MHN enable dual-mode imaging for cells *in vitro* and organs *in vivo* or *ex vivo*, combining the advantages of optical imaging (for microscopic resolution and *in vivo* fluorescent imaging) and MRI (for determination of full anatomical distribution *in vivo*). This approach may be applicable to the synthesis of other hybrid nanodevices that combine the dissimilar functions of two or more nanomaterials such as MRI, photo-thermal therapy, Raman imaging, and fluorescence imaging. Simultaneous dual-mode diagnosis and therapy with the hybrid system reported here may allow for more effective early detection and treatment of various types of cancers.

## Supplementary Material

Refer to Web version on PubMed Central for supplementary material.

## References

1. Harris TJ, Maltzahn GAv, Derfus AM, Ruoslahti E, Bhatia SN. *Angew. Chem.* 2006; 118:3233–3237. *Angew. Chem. Int. Ed.* 2006; 45:3161–3165.
2. Lee J-H, Jun Y-w, Yeon S-I, Shin J-S, Cheon J. *Angew. Chem.* 2006; 118:8340–8342. *Angew. Chem. Int. Ed.* 2006; 45:8160–8062.
3. Kim J, Park S, Lee JE, Jin SM, Lee JH, Lee IS, Yang I, Kim J-S, Kim SK, Cho M-H, Hyeon T. *Angew. Chem.* 2006; 118:7918–7922. *Angew. Chem. Int. Ed.* 2006; 45:7754–7758.
4. Mulder WJM, Koole R, Brandwijk RJ, Storm G, Chin PTK, Strijkers GJ, Donega CdM, Nicolay K, Griffioen AW. *Nano Lett.* 2006; 6:1–6. [PubMed: 16402777]
5. Xu C, Xie J, Ho D, Wang C, Kohler N, Walsh EG, Morgan JR, Chin YE, Sun S. *Angew. Chem.* 2007; 120:179–182. *Angew. Chem. Int. Ed.* 2007; 47:173–176.
6. Zhang X, Brynda M, Britt RD, Carroll EC, Larsen DS, Louie AY, Kauzlarich SM. *J. Am. Chem. Soc.* 2007; 129:10668–10669. [PubMed: 17691792]
7. Derfus AM, Maltzahn Gv, Harris TJ, Duza T, Vecchio KS, Ruoslahti E, Bhatia SN. *Adv. Mater.* 2007; 19:3932–3936.
8. Huh Y-M, Lee E-S, Lee J-H, Jun Y-w, Kim P-H, Yun C-O, Kim J-H, Suh J-S, Cheon J. *Adv. Mater.* 2007; 19:3109–3112.
9. Choi JH, Nguyen FT, Barone PW, Heller DA, Moll AE, Patel D, Boppart SA, Strano MS. *Nano Lett.* 2007; 7:861–867. [PubMed: 17335265]
10. Wang D, He J, Rosenzweig N, Rosenzweig Z. *Nano Lett.* 2004; 4:409–413.
11. Yi DK, Selvan ST, Lee SS, Papaefthymiou GC, Kundaliya D, Ying JY. *J. Am. Chem. Soc.* 2005; 127:4990–4991. [PubMed: 15810812]
12. Kim J, Lee JE, Lee J, Yu JH, Kim BC, An K, Hwang C-H, Shin J-G, Park Y, Kim J, Hyeon T. *J. Am. Chem. Soc.* 2005; 128:688–689. [PubMed: 16417336]
13. Sathe TR, Agrawal A, Nie S. *Anal. Chem.* 2006; 78:5627–5632. [PubMed: 16906704]
14. Kim B-S, Taton TA. *Langmuir.* 2007; 23:2198–2202. [PubMed: 17279714]
15. Song E-Q, Wang G-P, Xie H-Y, Zhang Z-L, Hu J, Peng J, Wu D-C, Shi Y-B, Pang D-W. *Clin. Chem.* 2007; 53:2177–2185. [PubMed: 17962366]
16. Zebli B, Susha AS, Sukhorukov GB, Rogach AL, Parak WJ. *Langmuir.* 2005; 21:4262–4265. [PubMed: 16032831]
17. Beaune G, Dubertret B, Clement O, Vayssettes C, Cabuil V, Menager C. *Angew. Chem.* 2007; 119:5517–5520. *Angew. Chem. Int. Ed.* 2007; 46:5421–5424.
18. Dubertret B, Skourides P, Norris DJ, Noireaux V, Brivanlou AH, Libchaber A. *Science.* 2002; 298:1759–1762. [PubMed: 12459582]
19. Gao Z, Lukyanov AN, Singhal A, Torchilin VP. *Nano Lett.* 2002; 2:979–982.
20. Torchilin VP, Lukyanov AN, Gao Z, Papahadjopoulos-Sternberg B. *Proc. Natl. Acad. Sci. USA.* 2003; 100:6039–6044. [PubMed: 12716967]
21. Jain TK, Morales MA, Sahoo SK, Leslie-Pelecky DL, Labhasetwar V. *Mol. Pharm.* 2005; 2:194–205. [PubMed: 15934780]
22. Ai H, Flask C, Weinberg B, Shuai X, Pagel MD, Farrell D, Duerk J, Gao J. *Adv. Mater.* 2005; 17:1949–1952.
23. Nasongkla N, Bey E, Ren J, Ai H, Khemtong C, Guthi S-F, Chin JS, Sherry AD, Boothman DA, Gao J. *Nano Lett.* 2006; 6:2427–2430. [PubMed: 17090068]
24. Liu Z, Cai WB, He LN, Nakayama N, Chen K, Sun XM, Chen XY, Dai HJ. *Nat. Nanotech.* 2007; 2:47–52.
25. Mandal SK, Lequeux N, Rotenberg B, Tramier M, Fattaccioli J, Bibette J, Dubertret B. *Langmuir.* 2005; 21:4175–4179. [PubMed: 15835991]
26. Medintz IL, Uyeda HT, Goldman ER, Mattoussi H. *Nature Mater.* 2005; 4:435–446. [PubMed: 15928695]
27. Michalet X, Pinaud FF, Bentolila LA, Tsay JM, Doose S, Li JJ, Sundaresan G, Wu AM, Gambhir SS, Weiss S. *Science.* 2005; 307:538–544. [PubMed: 15681376]

28. Josephson L, Kircher MF, Mahmood U, Tang Y, Weissleder R. *Bioconjugate Chem.* 2002; 13:554–560.
29. Weissleder R, Kelly K, Sun EY, Shtatland T, Josephson L. *Nature Biotech.* 2005; 23:1418–1423.
30. Perez JM, Josephson L, O'Loughlin T, Högemann D, Weissleder R. *Nature Biotech.* 2002; 20:816–820.
31. Choi J-S, Jun Y-W, Yeon S-I, Kim HC, Shin J-S, Cheon J. *J. Am. Chem. Soc.* 2006; 128:15982–15983. [PubMed: 17165720]
32. Gu H, Zheng R, Zhang X, Xu B. *J. Am. Chem. Soc.* 2004; 126:5664–5665. [PubMed: 15125648]
33. Porkka K, Laakkonen P, Hoffman JA, Bernasconi M, Ruoslahti E. *Proc. Natl Acad. Sci. USA.* 2002; 99:7444–7449. [PubMed: 12032302]
34. Christian S, Pilch J, Akerman ME, Porkka K, Laakkonen P, Ruoslahti E. *J. Cell Biol.* 2003; 163:871–878. [PubMed: 14638862]
35. Akerman ME, Chan WCW, Laakkonen P, Bhatia SN, Ruoslahti E. *Proc. Natl Acad. Sci. USA.* 2002; 99:12617–12621. [PubMed: 12235356]
36. Reddy GR, Bhojani MS, McConville P, Moody J, Moffat BA, Hall DE, Kim G, Koo Y-EL, Woolliscroft MJ, Sugai JV, Johnson TD, Philbert MA, Kopelman R, Rehemtulla A, Ross BD. *Clin. Cancer Res.* 2006; 12:6677–6686. [PubMed: 17121886]
37. Henke E, Perk J, Vider J, Candia Pd, Chin Y, Solit DB, Ponomarev V, Cartegni L, Manova K, Rosen N, Benezra R. *Nature Biotech.* 2008; 26:91–100.
38. Weissleder R. *Nature Biotech.* 2001; 19:316–317.
39. Lukyanov AN, Gao Z, Mazzola L, Torchilin VP. *Pharm. Res.* 2002; 19:1424–1429. [PubMed: 12425458]
40. Ballou B, Lagerholm BC, Ernst LA, Bruchez MP, Waggoner AS. *Bioconjugate Chem.* 2004; 15:79–86.
41. Jain RK. *Annu. Rev. Biomed. Eng.* 1999; 1:241–263. [PubMed: 11701489]
42. Maeda H, Wua J, Sawaa T, Matsumurab Y, Horic K. *J. Controlled Release.* 2000; 65:271–284.

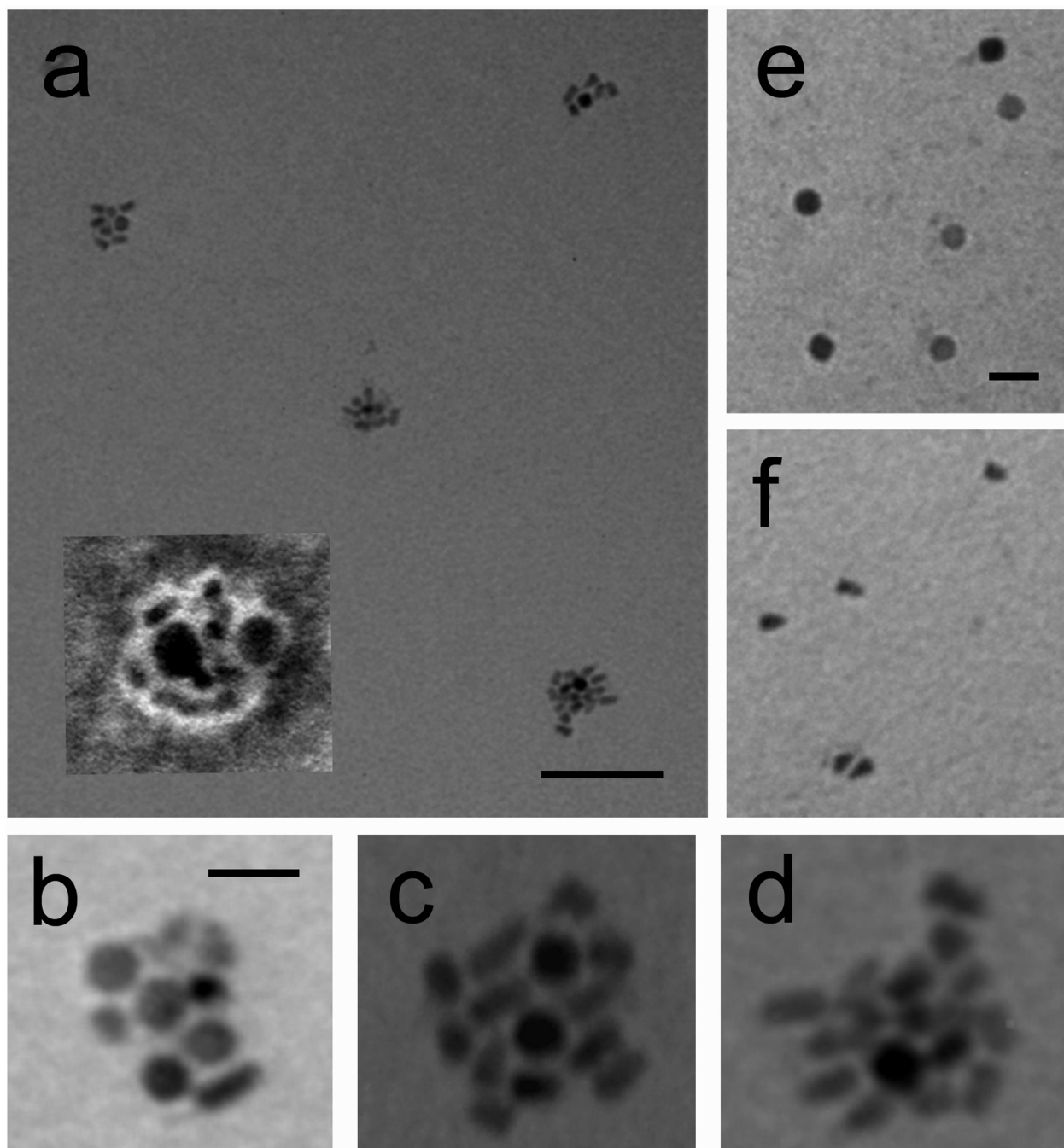


**Figure 1.**

Transmission electron microscope images of **a)** micellar hybrid nanoparticles (MHN) with a mass ratio of 1:5 magnetic nanoparticles (MN): quantum dots (QD) (inset: TEM image of an individual MHN that has been treated with a 1.3% phosphotungstic acid negative stain. The brighter regions are associated with the micellar coating). **b–d)** magnified images of MHN with a mass ratio of **b)** 1:1 MN:QD (MHN1); **c)** 1:3 MN:QD (MHN3); **d)** 1:5 MN:QD (MHN5). **e)** micellar magnetic nanoparticles. **f)** micellar quantum dots (emission  $\lambda_{\max} = 705$  nm). Scale bar in (a) is 100 nm. Scale bar in (b) is 20 nm; images (b–d) and the inset of (a) are displayed at the same magnification. Scale bar in (e) is 20 nm and (f) is displayed at the same magnification. In these formulations the QD have an elongated shape (2:1 aspect) and the MN are spherical.

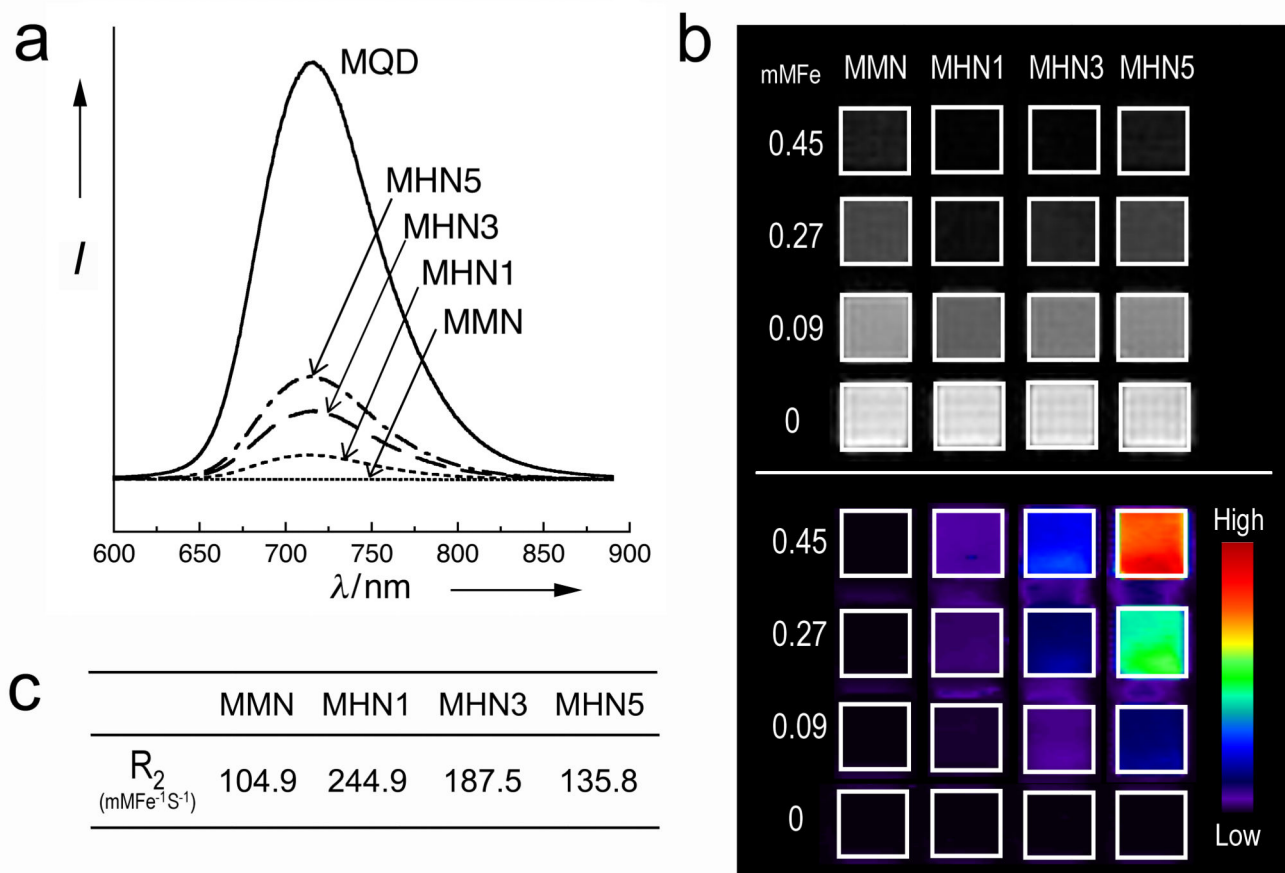


**Figure 2.**

a) Photoluminescence spectra of micellar quantum dots (MQD, emission  $\lambda_{\text{max}} = 705$  nm), micellar magnetic nanoparticles (MMN) and micellar hybrid nanoparticles (MHN) containing different ratios of MN:QD. The particle samples were excited with 450 nm light. The intensity ( $I$ ) of each spectrum is normalized by total mass of each particle type. b) Multimodal imaging of MMN and MHN as a function of iron concentration in MRI (upper panel,  $T_2$ -weighted mode) and NIR fluorescence (lower, in the Cy5.5 fluorescence channel,  $\lambda_{\text{ex}} = 680$  nm,  $\lambda_{\text{obs}} = 720$  nm). c) Relaxivity  $R_2$  values of MMN and MHN in the  $T_2$ -weighted MR images.

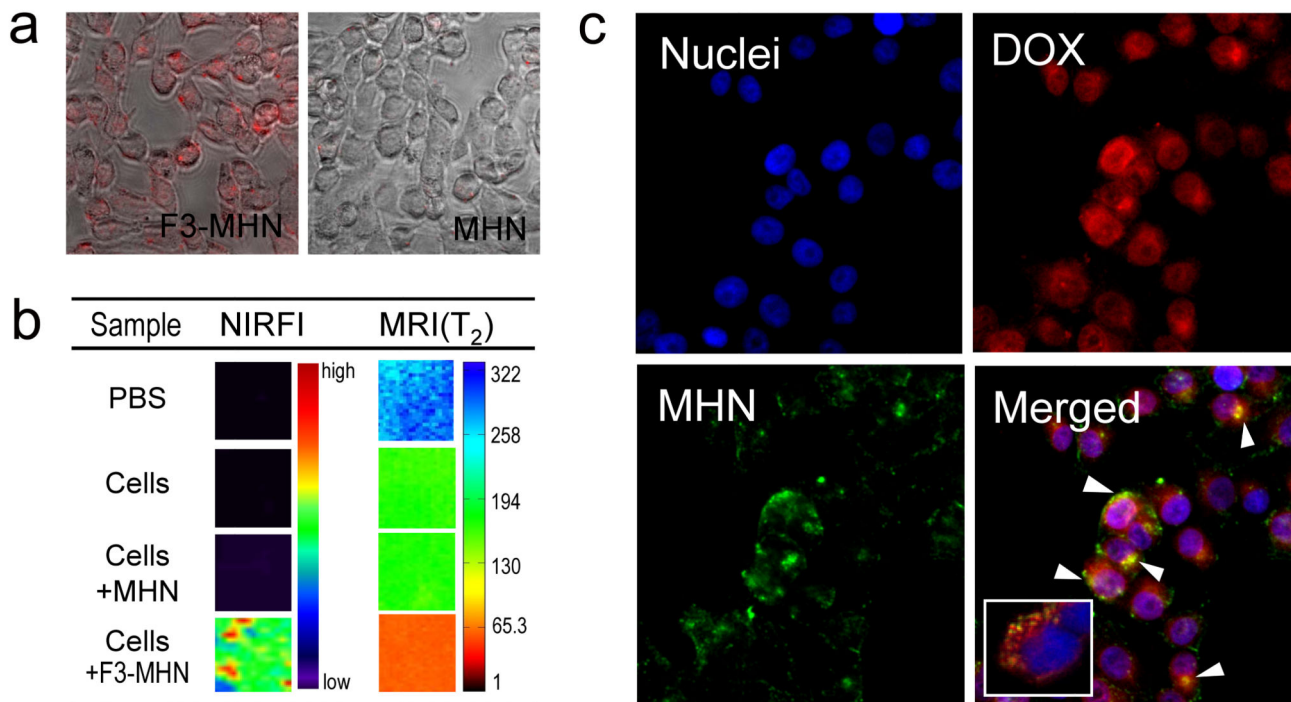


**Figure 3.**

a) Intracellular delivery of F3-conjugated micellar hybrid nanoparticles (F3-MHN) into MDA-MB-435 human carcinoma cells. In both panels the F3-MHN or the MHN control particles appear red in the images. 2 h after incubation with the cells, the F3-MHN particles are strongly associated with the cells, while the control nanoparticles (MHN) without the F3 species do not penetrate. b) Multimodal images (NIR fluorescence in Cy5.5 channel and MRI) of the cells in (a) compared with PBS control and with untreated cells. c) Targeted drug delivery of doxorubicin (DOX)-incorporated F3-MHN into MDA-MB-435 human carcinoma cells. The DOX-loaded F3-MHN were incubated with the cells for 2 h. Arrowheads indicate co-localization of DOX and MHN. The inset shows co-localization of some DOX (red) and endosome marker (green) 30 min after incubation with DOX-loaded F3-MHN. Nuclei were stained with DAPI.

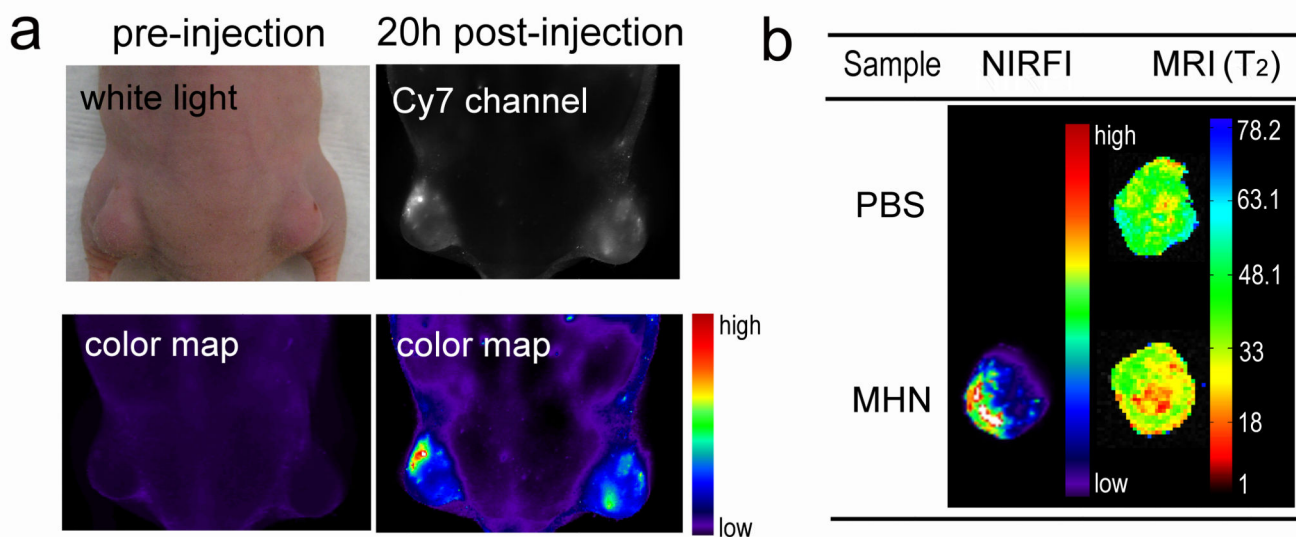


**Figure 4.**

**a)** NIR fluorescence images showing passive accumulation of micellar hybrid nanoparticles containing QD (emitting at 800 nm, MHN(800)) in a mouse bearing MDA-MB-435 tumors. The mouse was imaged pre-injection and 20 h post-injection (injection dose: 10 mg/kg). **b)** Image table representing multimodal imaging (by MRI and NIR fluorescence) of tumor harvested from the mouse in (a). PBS indicates a control in which a tumor-bearing mouse was injected with phosphate buffered saline. Column headings NIRFI and MRI(T<sub>2</sub>) indicate near-infrared fluorescence image and T<sub>2</sub> values from T<sub>2</sub>-weighted MRI, respectively.

